Simulation of Surface Acoustic Wave Devices

Sang Dae Yu

***Abstract*—The Mason crossed-field circuit model is generalized to simulate apodized interdigital transducers without channel division. The apodized transducer model is based on the transmission line model, and the artificial transformer with different voltage and current coupling ratios is used to independently obtain the transfer function and radiation admittance. In addition, a heuristic expression for transformer current ratios is used to approximate the radiation admittance of apodized transducers. Through comparing with the multichannel model, this unichannel model is illustrated to successfully describe the frequency response of apodized interdigital transducers.**

I. Introduction

Surface acoustic wave (SAW) devices have been widely used for television, radar, and wireless applications in the radio frequency (RF) ranges [1]. The simulation of such SAW devices in electronic circuits is very useful for system design and development. In particular, when SAW devices are connected to matching or peripheral circuits, the circuit effects like the insertion loss, the increase of sidelobe level, the passband flattening, and the triple transit echo (TTE) are involved. For the simulation of these effects, it is necessary to represent interdigital transducers (IDT) by equivalent circuit models compatible to the circuit simulator SPICE (Simulation Program with Integrated Circuit Emphasis) [2]. The Mason equivalent circuits for bulk acoustic wave (BAW) transducers have been widely used as approximate equivalent circuits for SAW IDTs [3]–[7]. In these models, the acoustic wave is represented by an electrical wave on a transmission line, and the piezoelectric energy conversion by a transformer. Moreover, the mechanical force and particle velocity at the acoustic ports are represented by equivalent voltage and current, respectively. As a result, the equivalent circuits for SAW IDTs have two symmetric acoustic ports and one electric port.

Until now, several circuit models for piezoelectric transducers have been developed for SPICE simulation. A simulation model of ultrasonic transducers has been implemented using a transmission line and an approximation of the negative capacitance in the Mason equivalent circuit [8]. Other simulation models for piezoelectric transducers have been developed using controlled-source analogous circuits [9]. The SPICE simulation for unapodized SAW interdigital transducers has been performed through the behavioral approximation of impedance elements in the Mason equivalent circuit by equivalent inductances and capacitances [10].

However, any SPICE model for apodized SAW interdigital transducers has not been reported yet, except a limited model [4], so apodized transducers mostly have been simulated using the multichannel model in which the transducer is divided into a large number of parallel channels [11]. Since each channel is regarded as a uniform IDT, a lot of computing time is required for long transducers. In this paper, the Mason crossed-field circuit model will be generalized to simulate apodized transducers without channel division. In this apodized transducer model, a SAW IDT is represented by a transmission line and the artificial transformers with the different voltage and current coupling ratios that are used to independently obtain the transfer function and radiation admittance. In order to illustrate the validity and usability of this unichannel model, the electrical characteristics for several SAW devices will be simulated and compared with those of the multichannel model widely accepted as a useful model.

II. Apodized Transducer Model

A. General Equivalent Circuit

The acoustic wave propagation in apodized SAW devices can be represented by a transmission line whose characteristic impedance Z_0 has the same value in the Mason equivalent circuits of all electrodes [4]. Here the apodization is realized by transformers with a single coupling ratio n proportional to the square root of overlap weighting. However, when the apodization varies appreciably like a sinc function, the analysis results of this limited model and multichannel model may differ significantly as shown in Fig. 1. To reduce such discrepancy, this model will be generalized by introducing two coupling ratios in the transformers. This unichannel model, of course, can be extended to include a wave impedance difference between the electroded and unelectroded sections.

The acoustic wave generated by the entire transducer is simply the sum of the contributions from each electrode pair. The acoustic beam width produced by an electrode pair is proportional to its overlap length. In the Mason circuit model, the acoustic beam width is related to the mechanical force. Therefore, the transformer ratio that converts from electrical signal to acoustical force needs to be proportional to the overlap length to correctly obtain the transfer function of apodized filters. In addition, the input admittance of the equivalent circuit should be equal to the radiation admittance of the transducer. In order to satisfy

Manuscript received July 1, 2003; accepted November 14, 2003.

The author is with Kyungpook National University, School of Electrical Engineering and Computer Science, Daegu, Republic of Korea (e-mail: sdyu@bh.knu.ac.kr).

0885–3010/$20.00 © 2004 IEEE

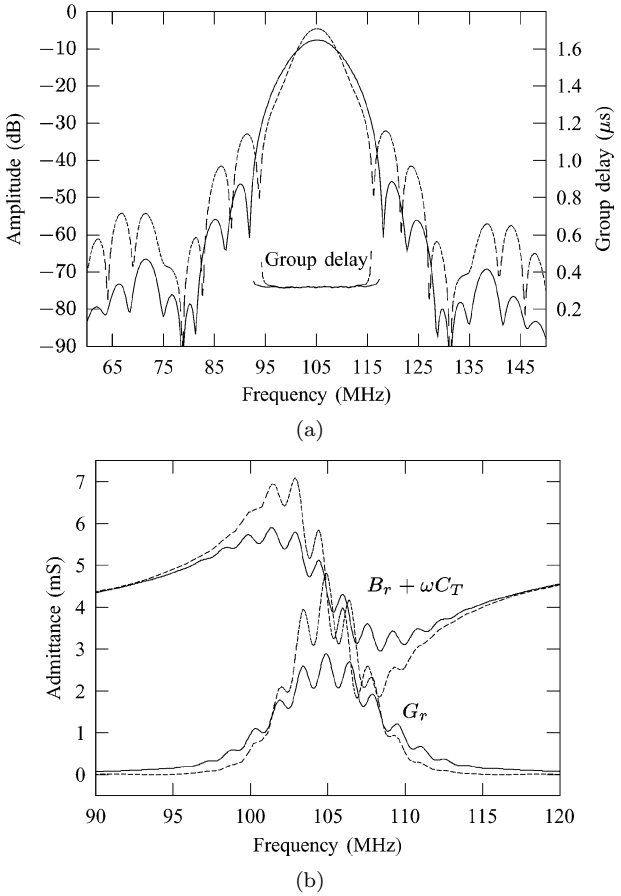

Fig. 1. Simulated frequency responses for an apodized SAW filter of Section III-D. Solid curve: by the multichannel model, dashed curve: by the limited model. (a) Transfer functions, (b) radiation admittances.

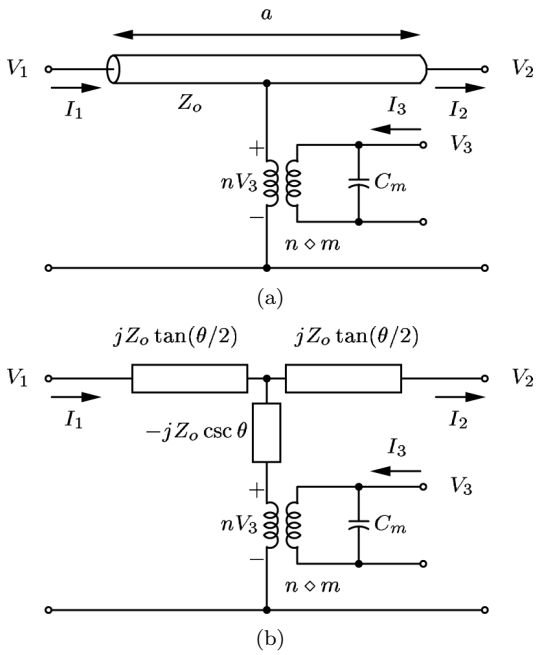

Fig. 2. General equivalent circuits based on the crossed-field circuit model for an electrode in the SAW interdigital transducer. n is the transformer voltage ratio and m is the transformer current ratio. (a) Transmission line model, (b) lumped element model.

these coupling conditions in apodized devices, it is necessary that two transformer ratios have appropriate values according to the coupling directions. As shown in Fig. 2, the one is the transformer voltage ratio n associated with the transfer function, the other is the transformer current ratio m associated with the input admittance.

The equations describing the general crossed-field circuit model shown in Fig. 2(a) can be written as

$$\begin{pmatrix} F_2 \\ I_2 \end{pmatrix} = \begin{pmatrix} \cos\theta & -jZ_0 \sin\theta \\ -jY_0 \sin\theta & \cos\theta \end{pmatrix} \begin{pmatrix} F_1 \\ I_1 \end{pmatrix}, \tag{1}$$

$$F_1 \equiv V_1 - nV_3,\ F_2 \equiv V_2 - nV_3, \tag{2}$$

$$m\,(I_1 - I_2) + I_3 = j\omega C_m V_3, \tag{3}$$

where θ is the transit angle of an electrode, $Y_0 \equiv 1/Z_0$ is the acoustic characteristic admittance, n is the transformer voltage ratio coupling electric voltage to acoustic force, m is the transformer current ratio coupling particle velocity to electric current, and $C_m = C_s/2$ is half the electrode capacitance. Furthermore, $Z_0 = \rho v_0 A_0$ and $\theta = \omega a/v_0$ where ρ is the mass density, v_0 is the wave velocity, A_0 is the wave area, and a is the electrode width. It can be shown that the transmission line is modeled as lumped circuit elements shown in Fig. 2(b). The relationship between the currents and voltages of this circuit can be described as the admittance matrix

$$\begin{pmatrix} I_1 \\ -I_2 \\ I_3 \end{pmatrix} = \begin{pmatrix} y_{11} & y_{12} & y_{13} \\ y_{12} & y_{11} & y_{13} \\ y_{31} & y_{31} & y_{33} \end{pmatrix} \begin{pmatrix} V_1 \\ V_2 \\ V_3 \end{pmatrix}, \tag{4}$$

where the admittance matrix elements are

$$y_{11} = -jY_0 \cot\theta,\ y_{12} = jY_0 \csc\theta, \tag{5}$$

$$y_{13} = -jnY_0 \tan(\theta/2),\ y_{31} = -jmY_0 \tan(\theta/2), \tag{6}$$

$$y_{33} = j2nmY_0 \tan(\theta/2) + j\omega C_m. \tag{7}$$

When a unit impulse is applied to the electric port and the acoustic ports are terminated in the characteristic impedance Z_0, the symmetrical responses at the acoustic ports

$$V_2 = V_1 = -Z_0 I_1 \tag{8}$$

will be obtained. Using (4) and (8), the transfer functions H_1 and H_2 are obtained as

$$H_1 \equiv \frac{V_1}{V_3} = jn \sin(\theta/2) e^{-j\theta/2} = H_2 \equiv \frac{V_2}{V_3}, \tag{9}$$

then the acoustic transfer function can be expressed as

$$H(j\omega) \equiv H_1 + H_2 = n\left(1 - e^{-j\theta}\right) = n\left(1 - e^{-j\omega\tau}\right), \tag{10}$$

where $\tau = a/v_0$. Using the inverse Fourier transform, the acoustic impulse response can be written as

$$h(t) = n[\delta(t) - \delta(t - \tau)], \tag{11}$$

where the origin of the time t is the left edge of the electrode. Thus, we can see that the equivalent circuit model in the frequency domain becomes equivalent to the delta function model in the time domain by making the transformer ratio n proportional to the overlap length w [12].

Generally, since the SAW energy is well confined within a Rayleigh wavelength from the surface of a piezoelectric substrate, the SAW propagation can be approximated by a homogeneous BAW with an effective wave area. Thus, the above BAW model can be applied to the SAW devices. The effective wave area is the effective cross-sectional area for the propagation of wave energy. For the SAW generated or detected by an electrode pair with overlap length w, the effective wave area can be written as

$$A = \lambda_0 w = \lambda_0 W \frac{w}{W} \equiv A_0 \frac{w}{W}, \tag{12}$$

where λ_0 is the wavelength at the synchronous frequency ω_0, and W is the aperture width of the IDT [13]. For an apodized IDT, the effective wave area of the electrode pair can be used to define the surface wave impedance Z_s as

$$Z_s = \rho v_0 A = \rho v_0 A_0 \frac{w}{W} \equiv Z_0 \frac{w}{W}. \tag{13}$$

Similarly, the static capacitance and radiation conductance of the electrode pair can be written as

$$C_s = C_a w = C_a W \frac{w}{W} \equiv C_0 \frac{w}{W}, \tag{14}$$

and

$$G_s = G_a w = G_a W \frac{w}{W} \equiv G_0 \frac{w}{W}, \tag{15}$$

where C_a and G_a are the static capacitance and radiation conductance of the electrode pair per unit aperture, respectively.

The transformer ratios can be determined by matching the radiation conductance and input conductance of one periodic section at the synchronous frequency [14]. The input conductance of one periodic section in the single-electrode transducer terminated with Y_0 can be obtained as

$$G_i = 8mnY_0 \sin^2(\theta/2) \sin^2(\theta/2 + \phi), \tag{16}$$

where ϕ is the transit angle of an unelectroded section and $\theta/2 + \phi = \pi/2$ at the synchronous frequency. By using the matching relation $G_i = G_s$ and the wave admittance $Y_s \equiv 1/Z_s$, the product of the transformer ratios can be arranged as

$$mn = \frac{G_s}{8Y_0}\csc^2(\theta/2) = \sqrt{\frac{G_s Y_s}{8Y_0^2}}\sqrt{\frac{G_s}{8Y_s}}\csc^2(\theta/2). \tag{17}$$

Thus, each of the transformer ratios is obtained as

$$m = \sqrt{\frac{G_s Y_s}{8Y_0^2}}\csc(\theta/2) = \sqrt{\frac{G_0}{8Y_0}}\csc(\theta/2), \tag{18}$$

$$n = \sqrt{\frac{G_s}{8Y_s}}\csc(\theta/2) = \frac{w}{W}\sqrt{\frac{G_0}{8Y_0}}\csc(\theta/2). \tag{19}$$

Here the transformer voltage ratio n is taken to be proportional to the overlap length w for correctly evaluating the transfer function of apodized filters. For unapodized transducers with $w = W$, two transformer ratios become equal like in conventional Mason circuit model. In apodized transducers, the spatial variation of wave energy occurs due to apodization, and the acoustic wave generated at a particular point interacts with only electrodes whose overlaps lie in its propagating path. Because the radiation conductance is dependent on such interactions, the modification of (15) obtained for uniform transducers is required to account for the apodization. As can be seen from (17), the modification to G_s can be achieved by refining m for the transformer voltage ratio n given by (19). Thus a heuristic expression for transformer current ratios of apodized devices has been found approximately and empirically through numerical experiments as

$$m_i = \alpha_0 \sin\left(\frac{\pi}{2} w_i\right) \sqrt{\frac{G_0}{8Y_0}}\csc(\theta/2), \tag{20}$$

for the case in which the input transducer has a sinc overlap, and the output transducer has a uniform overlap. Here α_0 is the matching factor for the radiation and input conductance of an apodized transducer at ω_0 and can be obtained as

$$\alpha_0 = \sum_{i=0}^{N-1} |c_i| \Big/ \sum_{i=0}^{N-1} \left|\sin\left(\frac{\pi}{2} w_i\right)\right| \sum_{i=0}^{N-1} |w_i|, \tag{21}$$

where w_i is the normalized overlap weighting and c_i is the overlap factor given in [15]. For the double-electrode transducer, the transformer ratios can be obtained as the ratios of (19) and (20) divided by $\sqrt{2}$, respectively.

B. Model Implementation

Through analysis for a multistrip coupler [16], the static capacitance C_a and radiation conductance G_a of one periodic section per unit aperture are given by

$$C_a = \sqrt{s/2}\,(\epsilon_0 + \epsilon_p)\,\frac{P_{-1/s}(\cos\eta\pi)}{P_{-1/s}(-\cos\eta\pi)}, \tag{22}$$

$$G_a = \frac{2\sqrt{2/s}\,\omega_0 C_a k^2}{P_{-1/s}(\cos\eta\pi) P_{-1/s}(-\cos\eta\pi)}, \tag{23}$$

for interdigital transducers [17] where s is the number of electrodes per electrical period, P_ν is the Legendre function with degree ν and may be evaluated using the expansion given in [18], η is the metalization ratio, k^2 is the piezoelectric coupling coefficient, and the permittivity ϵ_p is given by $\sqrt{\epsilon_{11}\epsilon_{33} - \epsilon_{13}\epsilon_{13}}$. This radiation conductance also has been derived by normal mode theory [19] and field analysis [20]. Fig. 3 shows the normalized conductances $G_n = G_a/\omega_0\,(\epsilon_0 + \epsilon_p)\,k^2$ and capacitances $C_n = C_a/\,(\epsilon_0 + \epsilon_p)$ as function of metalization ratio.

The electrodes in the SAW devices disturb the propagating SAW via the piezoelectric shorting effect and the

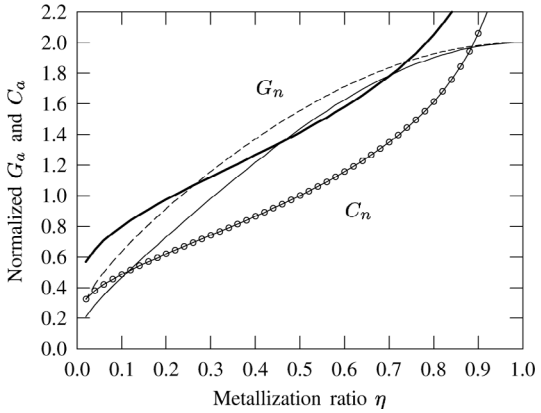

Fig. 3. Normalized conductances G_n and capacitances C_n as function of metalization ratio: solid curve for G_n of single electrodes; dashed curve for G_n of double electrodes; solid curve with circles for C_n of single electrodes; thick curve for C_n of double electrodes.

mechanical loading effect. These effects give rise to the internal reflection and the velocity shift of SAW. The internal reflection can be represented as the impedance mismatch in the transmission line model. The average velocity shift and impedance mismatch are given by

$$\frac{\Delta v}{v_0} = D_k\left(\frac{k^2}{2}\right) + D_m\left(\frac{h}{\lambda_0}\right) + D_s\left(\frac{h}{\lambda_0}\right)^2, \tag{24}$$

$$\frac{\Delta Z}{Z_0} = R_k\left(\frac{k^2}{2}\right) + R_m\left(\frac{h}{\lambda_0}\right), \tag{25}$$

where h is the electrode thickness [21]. The first terms represent the piezoelectric shorting effect, the second terms represent the mechanical loading effect, and the third term is the energy storage effect that reduces the velocity of SAW. The coefficients D_k, D_m, R_k, and R_m can be determined from the constants of substrate material, electrode material, and electrode geometry [22]. Generally, the average velocity shift and the impedance mismatch are characterized by the approximate polynomial expression, depending on the electrode width and thickness [23].

The reflection coefficient at an impedance discontinuity of a transmission line is defined as

$$\Gamma \equiv \frac{Y_0 - Y_x}{Y_0 + Y_x} \equiv \frac{Z_x - Z_0}{Z_x + Z_0} \simeq \frac{\Delta Z}{2Z_0}, \tag{26}$$

where the approximation is obtained with $|\Delta Z/Z_0| \ll 1$. Thus, this coefficient can be calculated directly from the impedance mismatch. When both the characteristic admittance perturbation and a shunt susceptance jB_r exist at the left edge of electrodes, the reflection coefficient is written as

$$\Gamma = \frac{Y_0 - Y_m - jB_r}{Y_0 + Y_m + jB_r} \simeq \frac{Y_0 - Y_m - jB_r}{2Y_0}, \tag{27}$$

where the approximation is obtained with $B_r/Y_0 \ll 1$. Hence, the surface impedance of the electroded sections and the shunt susceptance can be obtained as

$$Z_m = \frac{Z_0}{1 - \mathrm{Re}(2\Gamma^*)}, \tag{28}$$

$$B_r = Y_0 \mathrm{Im}(2\Gamma^*), \tag{29}$$

where Γ^* is the complex conjugate of Γ. For the case where $R_k = -1$ and $R_m = 0$, the surface impedance will be consistent with the expression $Z_0 = Z_m(1 + k^2/2)$ given in [4]. In addition, a negative susceptance $-jB_r$ at the right edge of electrodes is used to model the bilaterally asymmetric SAW devices [24]. These susceptances can be implemented approximately as a shunt capacitance C_r and a shunt inductance L_r at the synchronous frequency. The values of the capacitance and inductance are given by

$$C_r = \frac{B_r}{\omega_0}, \tag{30}$$

$$L_r = \frac{1}{\omega_0 B_r}. \tag{31}$$

In general, the synchronous frequency f_0 is determined by the average velocity of SAW. Using (24), the synchronous frequency is calculated as

$$f_0 = \frac{v_0}{2p}\left(1 + \frac{\Delta v}{v_0}\right), \tag{32}$$

where p is half the periodic length of the electrodes in the IDT. For the transmission line model of SPICE, the normalized electrical length of the electroded section is written as

$$\mathrm{NL} = \frac{\eta}{s}\frac{v_0}{v_m}. \tag{33}$$

In practice, it is desirable that the above equivalent circuit parameters are determined empirically or theoretically [25] to match the electrical responses of the actual transducer and the equivalent circuit.

The subcircuits for unelectroded and electroded sections are shown in Fig. 4 with modifiable parameters m, n, s, η, f_0, v_0, v_m, C_s, C_r, L_r, Z_0, and Z_m. The subcircuit `SAW` represents unelectroded sections in the interdigital transducer by a transmission line. The subcircuit `IDT` represents electroded sections by a transmission line, a voltage source for current measurement, two dependent sources for the artificial transformer, a capacitor and an inductor for asymmetrical devices, and a capacitor for the electrode capacitance.

III. Simulation of SAW Devices

In order to illustrate the usability and validity of the unichannel model, SPICE simulations are performed and compared for typical SAW devices such as unapodized transducers, apodized transducers, resonators, and filters.

A. Input Admittance for Unapodized Transducers

An unapodized, single-electrode transducer with $Y_m = Y_0$ is composed of N periodic sections whose acoustic ports

```
.subckt SAW 1 2 3
T0 1 3 2 3 Z0=Z0 F=f0 NL=(1-η)/s
.ends SAW

.subckt IDT 1 2 3 4 5
Tm 1 7 2 7 Z0=Zm F=f0 NL=η/(svm/v0)
Vm 7 6 0
Ev 6 3 4 5 n
Fi 5 4 Vm m
Cm 4 5 Cs/s
Cr 1 7 Cr
Lr 2 7 Lr
.ends IDT
```

Fig. 4. SPICE subcircuits for unelectroded and electroded sections in the SAW interdigital transducers.

are connected in cascade and electric ports are connected in parallel [3]. From circuit theory, this symmetrical transducer also is represented by an admittance matrix equation:

$$\begin{pmatrix} I_1 \\ I_2 \\ I_3 \end{pmatrix} = \begin{pmatrix} Y_{11} & Y_{12} & Y_{13} \\ Y_{12} & Y_{11} & -Y_{13} \\ Y_{13} & -Y_{13} & Y_{33} \end{pmatrix} \begin{pmatrix} V_1 \\ V_2 \\ V_3 \end{pmatrix}, \tag{34}$$

where the admittance matrix elements are

$$Y_{11} = -jY_0 \cot N(2\theta + 4\phi), \tag{35}$$

$$Y_{12} = jY_0 \csc N(2\theta + 4\phi), \tag{36}$$

$$Y_{13} = -jnY_0 \sin(\theta/2)/\cos(\theta/2 + \phi), \tag{37}$$

$$Y_{33} = j4n^2 N Y_0 \tan\frac{\theta}{2}\left[1 + \frac{\sin(\theta/2)\sin\phi}{\cos(\theta/2+\phi)}\right] + jN\omega C_s. \tag{38}$$

Using such elements, the input admittance of the unapodized transducer terminated with Y_0 can be calculated as

$$Y_i = Y_{33} + \frac{2Y_{13}^2}{Y_{12} - Y_{11} - Y_0} \equiv G_r + j(B_r + \omega C_T). \tag{39}$$

In Fig. 5, the calculated input admittance of the unapodized, single-electrode transducer without acoustic mismatch is compared with the input admittance simulated using SPICE. The calculated data exactly agree with the simulated symmetrical curves for the radiation admittance. This means that the transmission line model is equivalent to the lumped element model. From the simulation results for the transducer with acoustic mismatch, the admittance distortion due to acoustic reflection can be seen [26]. Moreover, it can be seen that the peak of the conductance is increased above the value obtained without mismatch [27], [28].

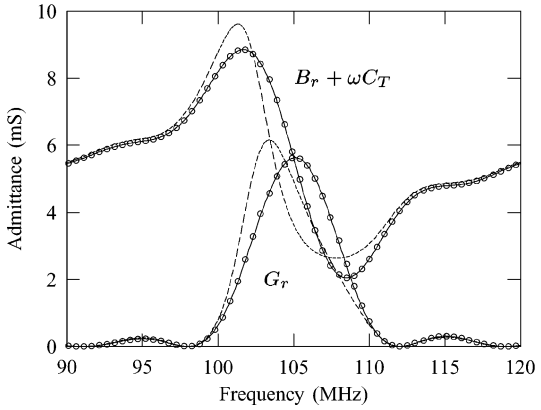

Fig. 5. Input admittances for an unapodized single-electrode transducer on YZ lithium niobate, with $N = 15$, $W = 1.25$ mm, $\eta = 0.5$, and $f_0 = 105$ MHz. The circles are the calculated data. Solid curves: with $Z_m = Z_0$; dashed curves: with $Z_m \neq Z_0$.

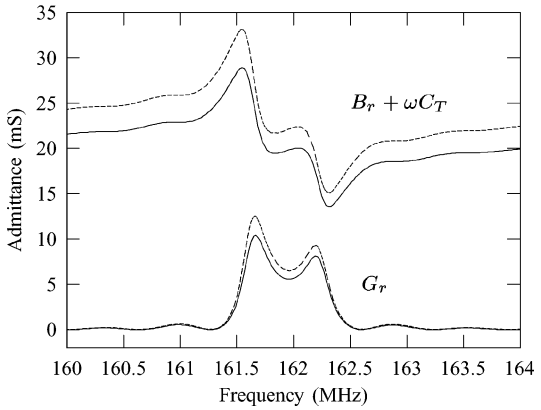

Fig. 6. Input admittances for an NSPUDT with $N = 250$, $W = 1.6$ mm, $\eta = 0.5$, and $\lambda_0 = 20$ μm on ST-cut 25°X-propagating quartz. Solid curve: without parasitics; dashed curve: with parasitics.

Fig. 6 shows the simulated radiation admittances of a natural single phase unidirectional transducer (NSPUDT) for which $C_r = 10.3$ pF and $L_r = 93.7$ nH. The solid curve is the input admittance simulated using the measured data [29] and the energy storage effect $D_s = 2\pi$; the dashed curve is the input admittance simulated, including the parasitics consisting of a 3.5-nH series inductance and a 0.8-pF parallel capacitance [7]. The radiation conductance has a dual peak. The left peak is the original peak distorted by acoustic reflection; the right peak is a new peak generated by the shunt susceptances for acoustic unidirectionality.

B. Input Admittance for Apodized Transducers

The radiation admittance of an apodized transducer usually is simulated with the multichannel method in which the transducer is divided into a number of unapodized transducers electrically connected in parallel [11]. In this method, the approximation is involved owing to the finite number of channels. Other methods to calculate the admittance of the apodized transducer are re-

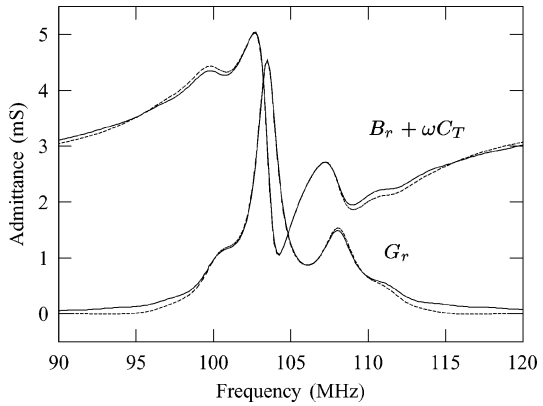

Fig. 7. Input admittances for an apodized single-electrode transducer with 64 aluminum electrodes on Y-cut, Z-propagating $LiNbO_3$. Solid curve: by the multichannel model; dashed curve: by the unichannel model.

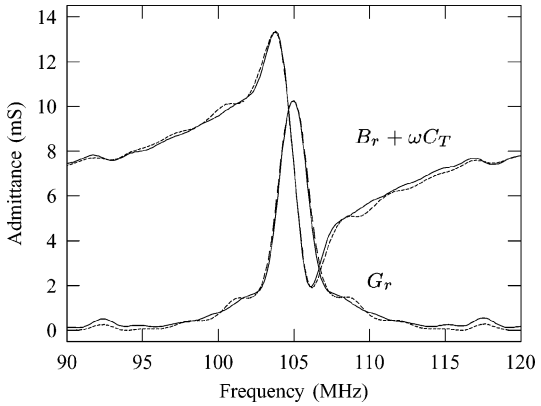

Fig. 8. Input admittances for an apodized double-electrode transducer with 256 aluminum electrodes on Y-cut, Z-propagating $LiNbO_3$. Solid curve: by the multichannel model; dashed curve: by the unichannel model.

ported [15], [30], [31]. In the unichannel model, the radiation admittance of the apodized transducer is also approximately simulated without channel division through the transformer current ratios given by (20). This model will be verified by comparing with the multichannel model for the radiation admittance.

Fig. 7 shows the simulated radiation admittances of an apodized transducer with 64 aluminum electrodes, $W = 1.25$ mm, $\eta = 0.5$, BW = 6%, and $\lambda_0 = 32.19$ μm on Y-cut Z-propagating lithium niobate ($LiNbO_3$) for which the coefficients of the velocity shift and the impedance mismatch are obtained from [32]. For the multichannel model, the transducer is divided into 100 channels. The apodization for this single-electrode transducer is realized by using the Blackman window function [33], then it is discretized so that each electrode end may correspond to the channel boundary for accuracy. The solid curve is the input admittance simulated using the multichannel model; the dashed curve is the input admittance simulated using the unichannel model. Although the admittance distortion due to acoustic reflection exists, it can be seen that there are relatively small differences in the radiation admittances.

Fig. 8 shows the simulated input admittances of an apodized, double-electrode transducer with 256 aluminum electrodes, $W = 1.25$ mm, $\eta = 0.5$, and $\lambda_0 = 32.19$ μm on Y-cut, Z-propagating $LiNbO_3$. For the multichannel model, the transducer is divided into 100 channels. The apodization is realized by only the sinc function without windowing, then it is discretized for the accuracy of the multichannel model. It can be seen that there are also small differences in the radiation admittances simulated using the unichannel and multichannel model.

C. Frequency Response of SAW Resonators

The SAW resonators have been used for low-power or low-loss wireless applications such as automotive keyless entry, remote control security, and wireless local area network (WLAN). In order to illustrate the simulation capability for these devices, the transfer function of a two-port, one-pole SAW resonator with shorted metal gratings has been simulated. Fig. 9 shows the simulated amplitude and phase responses of the resonator with five electrodes in each IDT and 100 electrodes in each grating on 36°YX lithium tantalate ($LiTaO_3$) for which the coefficients of the velocity shift and the impedance mismatch are obtained from [34]. Fig. 10 shows the simulated amplitude and phase responses of a two-port, one-pole SAW synchronous resonator. This device results in asymmetric response with slightly higher insertion loss as well as displacement of the resonant frequency dependent solely on the cavity length.

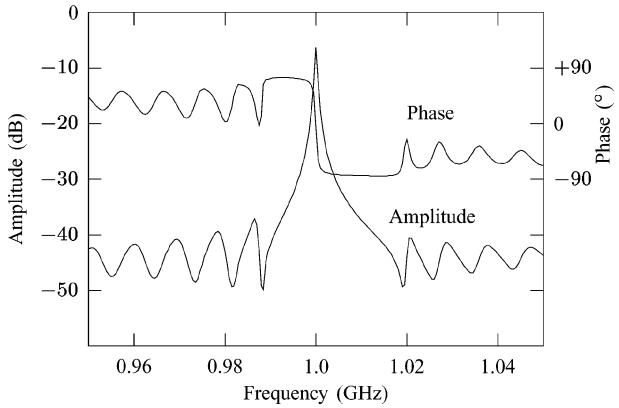

Fig. 9. Simulated amplitude and phase responses of a two-port, one-pole SAW resonator with five electrodes in each IDT, 100 electrodes in each grating, $W = 30\lambda_0$, $R_S = R_L = 50$ Ω, and $f_0 = 1$ GHz on 36°YX $LiTaO_3$.

D. Frequency Response of a SAW Filter

A SAW filter used in simulation consists of one apodized transducer and one uniform transducer. In order to reduce the passband distortion due to internal reflection, double-electrode transducers are used for both apodized and uniform transducers. Because an apodized or uniform transducer can be represented by a transversal filter, the same design principle can be used for this filter. The impulse

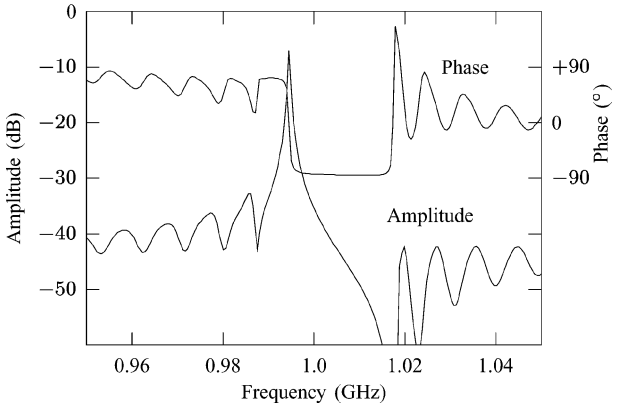

Fig. 10. Simulated amplitude and phase responses of a two-port, one-pole SAW synchronous resonator with five electrodes in each IDT, 100 electrodes in each grating, $W = 30\lambda_0$, and $R_S = R_L = 50\ \Omega$ on 36°YX $LiTaO_3$.

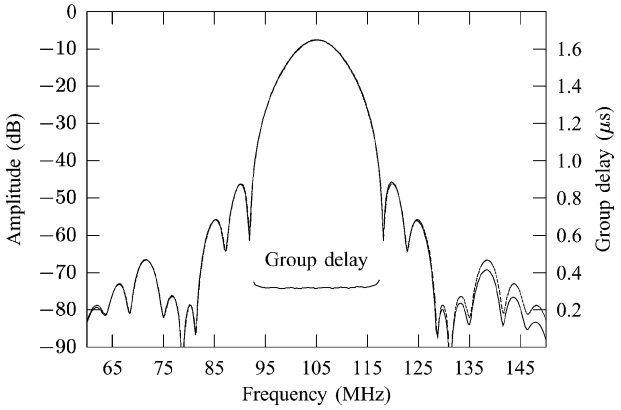

Fig. 11. Simulated amplitude and group delay responses of a SAW filter with apodized double-electrode input IDT, uniform double-electrode output IDT, $W = 1.25$ mm, $R_L = 2\ \text{k}\Omega$, and $f_0 = 105$ MHz on YZ $LiNbO_3$. Solid curve: by the multichannel and unichannel model; dashed curve: the ideal response calculated by FFT and shifted down by 7.6 dB for comparison.

response of the apodized transducer with 128 aluminum electrodes and 6% bandwidth has been designed using the Blackman window function and the delta function model [11], then it is also discretized for the accuracy of the multichannel model in which the filter is divided into 100 channels. The output transducer is the uniform transducer with 16 aluminum electrodes and a load resistor of 2 kΩ.

The simulated frequency responses of the unmatched SAW filter are shown in Fig. 11. The dashed curve is the ideal response calculated using the fast Fourier transform (FFT) and shifted down by 7.6 dB for comparison. The solid curves are the amplitude and group delay responses simulated using the unichannel model, which are identical with those simulated using the multichannel model. The total computing times on the 1-GHz Linux personal computer for the multichannel and unichannel model are 2202 and 3.9 seconds, respectively. It can be seen that there is good agreement with the ideal response, except for high-order sidelobes. The simulated input admittances of this

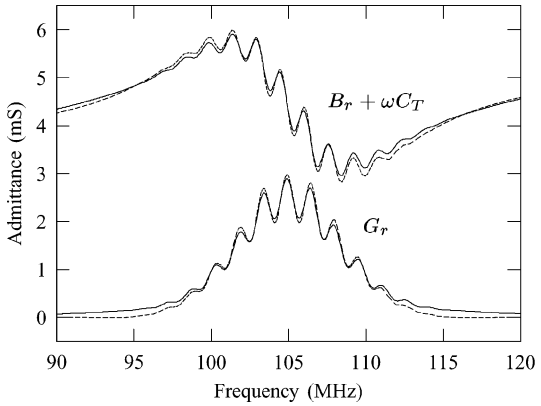

Fig. 12. Simulated radiation admittances of a SAW filter with apodized double-electrode input IDT, uniform double-electrode output IDT, $W = 1.25$ mm, $R_L = 2\ \text{k}\Omega$, and $f_0 = 105$ MHz on YZ $LiNbO_3$. Solid curve: by the multichannel model; dashed curve: by the unichannel model.

SAW filter are shown in Fig. 12. The solid curve is the input admittance simulated using the multichannel model; the dashed curve is the input admittance simulated using the unichannel model. It can be seen that there is also good agreement in the radiation admittances, except for slight differences in transition regions.

IV. Conclusions

A new equivalent circuit model has been used to simulate the SAW devices with an apodized IDT without channel division. In the apodized transducer model, a SAW IDT is represented by a transmission line and the artificial transformers with the different voltage and current coupling ratios that are used independently to obtain the transfer function and radiation admittance. A heuristic expression for transformer current ratios has been found to approximate the radiation admittance of an apodized IDT. Through comparison with the multichannel model, the validity and usability of the unichannel model has been illustrated for unapodized SAW transducers, apodized SAW transducers, SAW resonators, and SAW filters. From the successful results, the model can be used to design and simulate SAW devices with less computation effort.

References

[1] C. K. Campbell, *Surface Acoustic Wave Devices for Mobile and Wireless Communications*. New York: Academic, 1998, pp. 3–17.

[2] L. W. Nagel and D. O. Pederson, "SPICE: Simulation program with integrated circuit emphasis," Memo. No. UCB/ERL M382, Electronics Research Laboratory, University of California, Berkeley, Apr. 1973, unpublished.

[3] W. R. Smith, H. M. Gerard, J. H. Collins, T. M. Reeder, and H. J. Shaw, "Analysis of interdigital surface wave transducers by use of an equivalent circuit model," *IEEE Trans. Microwave Theory Tech.*, vol. 17, pp. 856–864, Nov. 1969.

[4] W. R. Smith, H. M. Gerard, and W. R. Jones, "Analysis and design of dispersive interdigital surface-wave transducers," *IEEE Trans. Microwave Theory Tech.*, vol. 20, pp. 458–471, July 1972.

[5] W. R. Smith, "Experimental distinction between crossed-field and in-line three-port circuit models for interdigital transducers," *IEEE Trans. Microwave Theory Tech.*, vol. 22, pp. 960–964, Nov. 1974.
[6] R. F. Milsom and M. Redwood, "Interdigital piezoelectric Rayleigh wave transducer: An improved equivalent circuit," *Electron. Lett.*, vol. 7, pp. 217–218, May 1971.
[7] M. P. da Cunha and E. L. Adler, "A network model for arbitrarily oriented IDT structures," *IEEE Trans. Ultrason., Ferroelect., Freq. Contr.*, vol. 40, pp. 622–629, Nov. 1993.
[8] S. A. Morris and C. G. Hutchens, "Implementation of Mason's model on circuit analysis programs," *IEEE Trans. Ultrason., Ferroelect., Freq. Contr.*, vol. 33, pp. 295–398, May 1986.
[9] W. M. Leach, "Controlled-source analogous circuits and SPICE models for piezoelectric transducers," *IEEE Trans. Ultrason., Ferroelect., Freq. Contr.*, vol. 41, pp. 60–66, Jan. 1994.
[10] A. B. Bhattacharyya, S. Tuli, and S. Majumdar, "SPICE simulation of surface acoustic wave interdigital transducers," *IEEE Trans. Ultrason., Ferroelect., Freq. Contr.*, vol. 42, pp. 784–786, July 1995.
[11] R. H. Tancrell and M. G. Holland, "Acoustic surface wave filters," *Proc. IEEE*, vol. 59, pp. 393–409, Mar. 1971.
[12] H. M. Gerard, "Principles of surface wave filter design," in *Acoustic Surface Waves*. A. A. Oliner, Ed. New York: Springer-Verlag, 1978, pp. 61–96.
[13] V. M. Ristic, *Principles of Acoustic Devices*. New York: Wiley, 1983, pp. 250–255.
[14] T. Shiba, J. Yamada, and A. Yuhara, "Transformer ratio and capacitance in general form for equivalent circuit of SAW IDTs," in *Proc. IEEE Ultrason. Symp.*, Dec. 1991, pp. 101–105.
[15] P. J. Naglowski, "Fast computation of finger-length-weighted SAW transducer dynamic admittance," *Electron. Lett.*, vol. 24, pp. 1494–1496, Nov. 1988.
[16] H. Engan, "Surface acoustic wave multielectrode transducers," *IEEE Trans. Sonics Ultrason.*, vol. 22, pp. 395–401, Nov. 1975.
[17] K. Hashimoto, *Surface Acoustic Wave Devices in Telecommunications*. New York: Springer-Verlag, 2000, pp. 52–85.
[18] D. P. Morgan, *Surface-Wave Devices for Signal Processing*. Amsterdam: Elsevier, 1985, pp. 355–358.
[19] B. A. Auld and G. S. Kino, "Normal mode theory for acoustic waves and its application to the interdigital transducer," *IEEE Trans. Electron Devices*, vol. 18, pp. 898–908, Oct. 1971.
[20] R. F. Milsom, M. Redwood, and N. H. C. Reilly, "The interdigital transducer," in *Surface Wave Filters*. H. Matthews, Ed. New York: Wiley, 1977, pp. 55–108.
[21] T. Thorvaldsson, "Analysis of the natural single phase unidirectional SAW transducer," in *Proc. IEEE Ultrason. Symp.*, Oct. 1989, pp. 91–96.
[22] S. Datta, *Surface Acoustic Wave Devices*. Englewood Cliffs, NJ: Prentice-Hall, 1986, pp. 151–178.
[23] K. Ibata, T. Omori, K. Hashimoto, and M. Yamaguchi, "Polynomial expression for SAW reflection by aluminum gratings on 128°YX-$LiNbO_3$," in *Proc. IEEE Ultrason. Symp.*, 1998, pp. 193–197.
[24] E. L. Adler, M. P. da Cunha, and O. Schwelb, "Arbitrarily oriented SAW gratings: Network model and the coupling-of-modes description," *IEEE Trans. Ultrason., Ferroelect., Freq. Contr.*, vol. 38, pp. 220–230, May 1991.
[25] K. Inagawa and M. Koshiba, "Equivalent networks for SAW interdigital transducers," *IEEE Trans. Ultrason., Ferroelect., Freq. Contr.*, vol. 41, pp. 402–411, May 1994.
[26] M. R. Daniel and P. R. Emtage, "Distortion of the central resonance in long interdigital transducers," *Appl. Phys. Lett.*, vol. 20, pp. 320–322, Apr. 1972.
[27] W. S. Jones, C. S. Hartmann, and T. D. Sturdivant, "Second order effects in surface wave devices," *IEEE Trans. Sonics Ultrason.*, vol. 19, pp. 368–377, July 1972.
[28] G. L. Matthaei, D. Y. Wong, and B. P. O'Shaughnessy, "Simplifications for the analysis of interdigital surface-wave devices," *IEEE Trans. Sonics Ultrason.*, vol. 22, pp. 105–114, Mar. 1975.
[29] T. Thorvaldsson and B. P. Abbott, "Low loss SAW filters utilizing the natural single phase unidirectional transducer (NSPUDT)," in *Proc. IEEE Ultrason. Symp.*, Dec. 1990, pp. 43–48.
[30] D. P. Morgan, "Admittance calculations for non-reflective SAW transducers," in *Proc. IEEE Ultrason. Symp.*, Nov. 1996, pp. 131–134.
[31] W. Soluch, "Admittance matrix of a surface acoustic wave interdigital transducer," *IEEE Trans. Ultrason., Ferroelect., Freq. Contr.*, vol. 40, pp. 828–831, Nov. 1993.
[32] D. P. Chen and H. A. Haus, "Analysis of metal-strip SAW gratings and transducers," *IEEE Trans. Sonics Ultrason.*, vol. 32, pp. 395–408, May 1985.
[33] A. V. Oppenheim and R. W. Schafer, *Digital Signal Processing*. Englewood Cliffs, NJ: Prentice-Hall, 1975, pp. 237–250.
[34] T. Morita, Y. Watanabe, M. Tanaka, and Y. Nakazawa, "Wideband low loss double mode SAW filters," in *Proc. IEEE Ultrason. Symp.*, Oct. 1992, pp. 95–104.

Sang Dae Yu was born in Ulsan, Korea on February 12, 1958. He received the B.S. degree in electronic engineering from Kyungpook National University, Korea in 1980, and the M.S. and Ph.D. degrees in electrical engineering from Korea Advanced Institute of Science and Technology, Korea in 1982 and 1998, respectively. Since 1982, he has been with the School of Electrical Engineering and Computer Science, Kyungpook National University, where he is now a Professor. His current interests include integrated circuit design, design automation, device modeling, SAW filters, and embedded systems. Prof. Yu is a member of the Institute of Electronics Engineers of Korea and the Korean Sensors Society.